Teamwork in the viscous oceanic microscale

Eva A. Kanso[a,1], Rubens M. Lopes[b], J. Rudi Strickler[c,d], John O. Dabiri[e], and John H. Costello[f,g,1]

[a]Department of Aerospace and Mechanical Engineering, University of Southern California, Los Angeles, CA 90089; [b]Departamento de Oceanografia Biológica, Instituto Oceanográfico, Universidade de São Paulo, São Paulo 05508-120 Brazil; [c]Department of Biological Sciences, University of Wisconsin–Milwaukee, Milwaukee, WI 53204; [d]Marine Science Institute, University of Texas at Austin, Port Aransas, TX 78373; [e]Graduate Aerospace Laboratories and Mechanical Engineering, California Institute of Technology, Pasadena, CA 91125; [f]Biology Department, Providence College, Providence, RI 02918; and [g]Whitman Center, Marine Biological Laboratory, Woods Hole, MA 02543

Edited by David M. Karl, University of Hawai'i at Mānoa, Honolulu, HI, and approved June 1, 2021 (received for review August 27, 2020)

Nutrient acquisition is crucial for oceanic microbes, and competitive solutions to solve this challenge have evolved among a range of unicellular protists. However, solitary solutions are not the only approach found in natural populations. A diverse array of oceanic protists form temporary or even long-lasting attachments to other protists and marine aggregates. Do these planktonic consortia provide benefits to their members? Here, we use empirical and modeling approaches to evaluate whether the relationship between a large centric diatom, *Coscinodiscus wailesii*, and a ciliate epibiont, *Pseudovorticella coscinodisci*, provides nutrient flux benefits to the host diatom. We find that fluid flows generated by ciliary beating can increase nutrient flux to a diatom cell surface four to 10 times that of a still cell without ciliate epibionts. This cosmopolitan species of diatom does not form consortia in all environments but frequently joins such consortia in nutrient-depleted waters. Our results demonstrate that symbiotic consortia provide a cooperative alternative of comparable or greater magnitude to sinking for enhancement of nutrient acquisition in challenging environments.

phytoplankton | nutrient limitation | symbiosis | diffusion limitation | cell size

Global models of oxygen and carbon dioxide alterations depend upon transfer rates between small phytoplankton cells and surrounding surface waters of the world's oceans (1–3). Although these cells are important on large scales, their individual interactions occur at microscopic dimensions that are dominated by viscosity. In this viscous environment, critical cellular processes, such as the exchange of nutrients, metabolites, and wastes, rely upon diffusion (4). While diffusion is an effective means of nutrient transport for the smallest microbes (5), it also creates a depleted region around the cell surface, referred to as the diffusion boundary layer (DBL), that limits nutrient consumption and cell growth (6, 7). The DBL for a cell at rest extends nine cell radii from the cell surface before the nutrient concentration reaches 90% of ambient levels (8), creating formidable disadvantages for nutrient acquisition by large cells requiring nutrient diffusion across large distances relative to their cell size (9). Phytoplankton have evolved mechanisms to mitigate the limitations of diffusive transfer rates by swimming or sinking (10) to generate relative motion between the cell and surrounding fluid. Diatoms—barrel-shaped, nonmotile eukaryotes—are considered to be one of the most ecologically important groups of phytoplankton (11–14) that absorb nutrients across their whole cell surface (15) but often increase sinking rates when experiencing nutrient limitation (16). Sinking thins the DBL surrounding the diatom cell and reduces the distance over which diffusion limits nutrient transport (8, 17). One potential disadvantage of this mechanism for DBL reduction is the high probability for a cell to sink out of sunlit regions, and sinking diatoms are major contributors to organic mass flux from surface to deep oceanic waters (1). A widespread but unevaluated alternative for such large cells involves teamwork with other smaller, motile cells that combine to form multicell consortia. Consortia are typically comprised of larger nonmotile host cells with smaller, surface-adhering motile cells termed epibionts. Although infrequently studied, epibionts are ubiquitous in the micrometer-scale world of planktonic organisms (18), and flagellated or ciliated epibionts often attach to larger objects (19) or marine snow (20). The selective forces favoring epibiont attachment remain in question. A range of fluid dynamic effects on prey encounter as well as biological factors such as reduced predator encounter risk or elevated prey availability surrounding host attachment sites have been proposed to explain the widespread nature of epibiont attachment (21, 22). However, the movement of motile epibiont cilia or flagella alters flows and, hence, creates an altered fluid dynamic environment surrounding the consortia. What are the consequences for the consortium host—does a larger, nonmotile cell benefit by membership in consortia? While advantages to the epibiont have been examined, the impacts on the host cells within a consortium have remained largely unconsidered. One reason for this is that physical associations between members of consortia are often temporary, and the short time scales of these relationships have hampered direct evaluation of the fluid mechanical interactions between consortium members.

Here, we describe experimental work in combination with mathematical models that quantify the effect of the epibiont's advective currents on nutrient availability to host cells within consortia formed by a large diatom, *Coscinodiscus wailesii*, and its peritrich ciliate epibiont, *Pseudovorticella coscinodisci* (Fig. 1*A*). Consortia composed of *C. wailesii* and *P. coscinodisci* are common along the Atlantic coast of South America (23, 24) and have provided a valuable opportunity for measuring fluid interactions characterizing a planktonic host–epibiont association.

Significance

Nutrient acquisition is a challenge that often favors small individual phytoplanktors because they are superior competitors at low nutrient levels. An alternative to these individual solutions is the union of different species into consortia that rely upon division of labor for competitive advantage. Although planktonic epibionts are well documented, the advantages of consortia for the larger host cells have remained unclear. Here, we demonstrate that attached ciliates dramatically increase the flux of dissolved nutrients to host phytoplankton cells, providing the necessary conditions for large diatoms to thrive in oligotrophic ecosystems. This demonstrates that unions between different species can substantially increase rates of nutrient flow to host cells and provides an alternative to sinking for protists living in low-nutrient conditions.

Author contributions: R.M.L., J.R.S., and J.H.C. designed research; R.M.L., J.R.S., and J.H.C. performed research; E.A.K., J.O.D., and J.H.C. contributed new analytic tools; E.A.K., R.M.L., J.R.S., J.O.D., and J.H.C. analyzed data; and E.A.K., R.M.L., and J.H.C. wrote the paper.

The authors declare no competing interest.

This article is a PNAS Direct Submission.

[1]To whom correspondence may be addressed. Email: costello@providence.edu or kanso@usc.edu.

This article contains supporting information online at https://www.pnas.org/lookup/suppl/doi:10.1073/pnas.2018193118/-/DCSupplemental.

Published July 16, 2021.

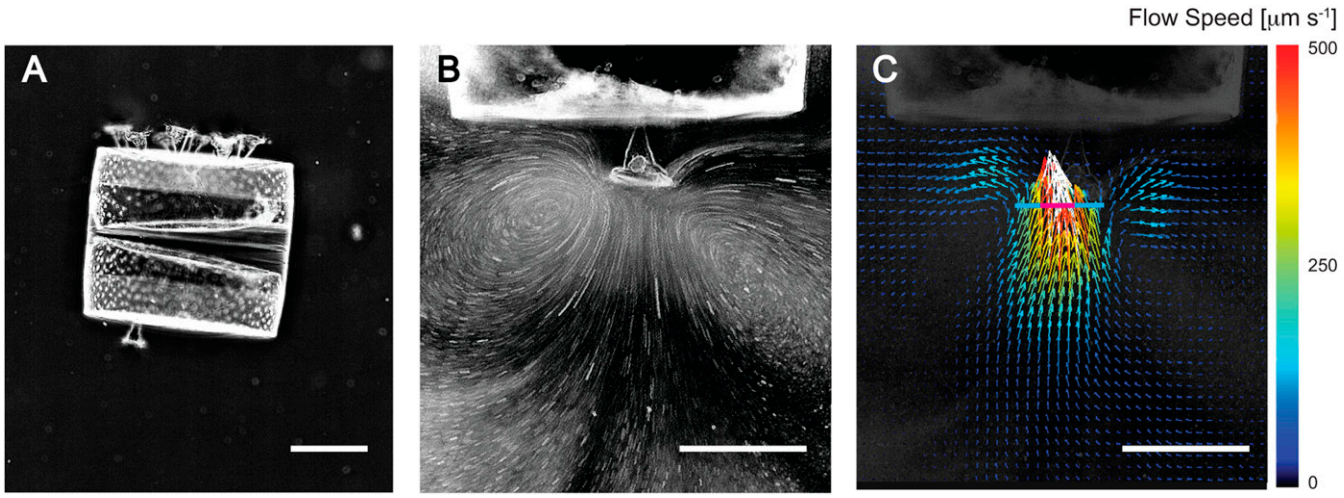

Fig. 1. Diatom–ciliate association: (*A*) diatom *C. wailesii* and its epibiont *P. coscinodisci*. Scale bars represent 100 microns in length. (*B*) Flow around a single ciliate directed toward the diatom cell surface. (*C*) Velocity field for the same diatom–ciliate pair with a blue line indicating the transect line used for measurement of flow field velocities. The magenta segment represents the microcurrent component that directly intercepts the ciliary crown.

Results

Epibiont-Generated Flows. The ciliate *P. coscinodisci*, when attached to *C. wailesii*, generated flows that entrained fluid toward the diatom along the direction normal to its surface and then around the diatom body (Fig. 1 *B* and *C* and *SI Appendix*, Movies S1–S3). Particle image velocimetry (PIV) transects demonstrated that the microcurrent speeds were maximal near the center of the ciliary crown and decreased away from the crown, at times forming small viscous eddies on either side of the ciliary crown (Fig. 1 *B* and *C*), that became exaggerated when near the fluorodish wall (*SI Appendix*, Movie S1). Eddies characterize feeding currents near infinitely-long flat walls and could limit the benefits of advective nutrient transport by recirculating fluid past the ciliate feeding apparatus after nutrients have been removed (25, 26). We observed a recirculation component within the consortium flow (Fig. 1*B*), but the limited diatom cell surface allowed substantial flow past the epibiont and along the diatom cell body (Fig. 2*A* and *SI Appendix*, Movies S1 and S5). Surface geometry is an important determinant of viscous eddy recirculation for attached ciliates (25, 27), and the finite diatom body minimized recirculation of advected fluid within viscous eddies for *Coscinodiscus–Pseudovorticella* consortia. Additionally, ciliate feeding currents generated forces and torques capable of altering the consortia's motion as well as orientation in the fluid (*SI Appendix*, Movie S5). Such whole-consortia movements can disrupt eddy formation compared to infinite, static surfaces. Such disruptions caused by whole-consortia rotations may introduce fresh fluid—and nutrients—to the consortia (28, 29).

Due to compression of fluid streamlines near the ciliated crown (30), the portion of the microcurrent entering the ciliary feeding region, and therefore eligible for clearing prey particles (31), was about half of the total microcurrent flow (46%, SD = 3.1%, $n = 8$ ciliates). Much of the microcurrent flow (54%) did not enter the ciliary crown region but passed to either side of the ciliate, potentially transporting fresh nutrient-laden fluid to the diatom surface. Indeed, the fluid entering the crown exited as an excurrent flow that was distinct, relative to the fluids that did not pass through the ciliary crown (*SI Appendix*, Movies S2–S4). Flow velocities entering the ciliary crown reached values of U ≥ 500 μm·s^{-1}, with average maximum = 496, SD = 59 μm·s^{-1}, and mean across ciliary crown = 362, SD = 44 μm·s^{-1}, for $n = 8$ ciliate–host replicates (Fig. 1*C*). These flows are of similar velocities to those measured for peritrich

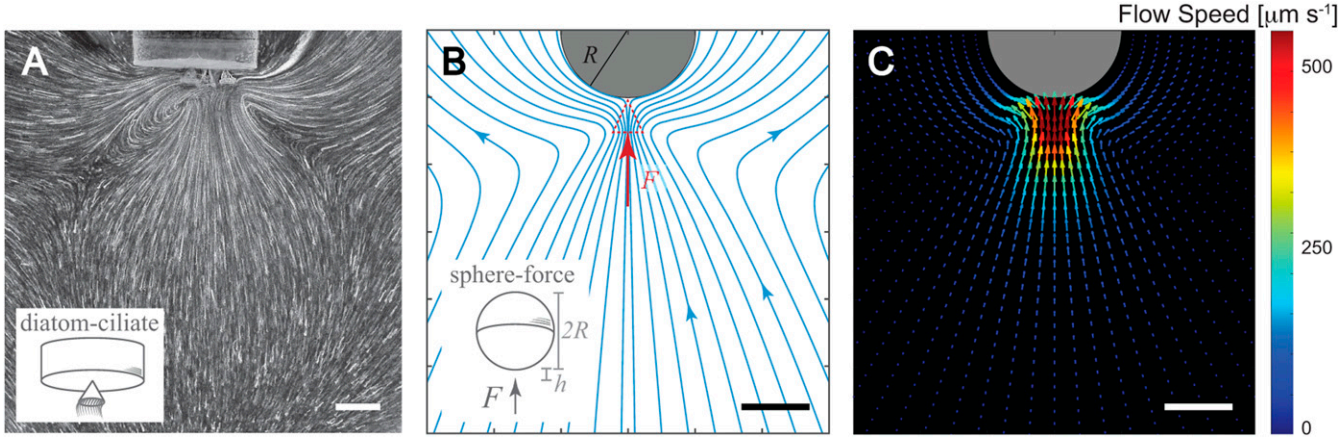

Fig. 2. Diatom–ciliate model: (*A*) Streamlines of particle paths generated by the flow field of a three-member cluster of the ciliate *P. coscinodisci* attached to the diatom *C. wailesii*. (*B*) Streamlines produced by the diatom–ciliate model consisting of a sphere of radius R and a regularized Stokeslet of dimensionless strength F = 10 and regularization parameter $r = 0.4$ R located at a distance h = 0.5 R from the sphere's south pole and pointing toward the sphere's center. (*C*) Velocity field for the same diatom–ciliate model. Scale bars represent 100 microns in length.

ciliates within the frequently studied genus *Vorticella* (31, 32) as well as ephemerally attached heterotrophic flagellates (300 to 400 $\mu m \cdot s^{-1}$ (19). By approximating the cell volume of a *P. coscinodisci* ciliate (average height 44.2 μm ± 6.2 μm, base 40.5 μm ± 4.9 μm, volume 19,524.6 μm^3 ± 6,786.4 μm^3, $n = 58$ individuals, *SI Appendix*, Fig. S5 and Table S7), we estimate the average volume transported to the ciliated crown feeding surfaces, and therefore eligible for clearing prey particles, of an individual, attached *P. coscinodisci* ciliate to be $\sim 1.8 \times 10^5$ body volumes$\cdot h^{-1}$. Total flow, including fluid not passing through the ciliary crown, was $\sim 3.8 \times 10^5$ body volumes$\cdot h^{-1}$. Both values fall well within volume-specific clearance rate estimates for other protists that range between 10^4 and 10^6 body volumes$\cdot h^{-1}$ of prey particles (*SI Appendix*, Table S6), indicating that the microcurrent traits that we measured for the *Coscinodiscus–Pseudovorticella* consortia are representative of other protists living in a variety of aquatic environments.

Benefits of Epibiont-Generated Flows to the Diatom Host. We predicted that the presence of microcurrents would accelerate solute transport to and from the diatom host. These consortia were isolated from surface oligotrophic waters in which nutrient availability would be expected to constrain diatom growth (33). Small molecules, such as oxygen and dissolved silica with diffusivities that are in the order of $D = 10^{-9}$ $m^2 \cdot s^{-1}$, when transported by the observed flows, traverse a distance R (the cell radius) = 100 μm at a speed U = 100 $\mu m \cdot s^{-1}$ in approximately R/U = 1 s. In contrast, solutes transported by diffusion alone take a considerably longer time, R^2/D = 10 s, to traverse the same distance. The ratio of diffusive to advective timescales is measured by the Péclet number (Pe = UR/D). When Pe << 1, mass transport is controlled by molecular diffusion. For the range of speeds that we observed, we obtain Pe = 10 to 50, implying that advection dominated even the slowest epibiont flows that we recorded (*SI Appendix*, Tables S1 and S2). This dimensional analysis suggests that the flows generated by the ciliate epibiont substantially enhance the transport of solutes to and from the diatom surface.

Quantifying Nutrient Availability to the Diatom. To quantify the benefits of the epibiont-induced flows to the diatom, we developed a mathematical model that allows comparison of the corresponding nutrient flux to i) diffusive flux and ii) flux to a sinking diatom. The model (*SI Appendix*) approximated the diatom by a sphere of radius R and subsumed traits of the ciliate flow into a single averaged parameter—the force F that the ciliate exerts on the fluid. Dimensional analysis shows that this force scales as $F = \eta U R_{ciliate}$, where $\eta = 10^{-3}$ $kg \cdot m^{-1} \cdot s^{-1}$ is the viscosity of seawater. For an individual ciliate, $R_{ciliate}$ = 20 μm and U = 100 to 500 $\mu m \cdot s^{-1}$, F = 2 to 10 pN (*SI Appendix*, Table S1).

The fluid velocity u created by the ciliate vanishes at the surface of the diatom and decays to zero far from the diatom surface. Because inertia is unimportant at this scale, u must satisfy the Stokes equation $\nabla P = \eta \Delta \mathbf{u}$, where p is pressure; it must also be incompressible $\nabla \cdot \mathbf{u} = 0$. We solved these equations analytically to obtain the velocity field u generated by a regularized Stokeslet force, emulating the effect of the epibiont ciliated crown, located at a distance h/R from the diatom surface and pointing toward the center of the diatom (34). Although not an exact replica of empirically measured flows, the three-dimensional flow field of the regularized Stokeslet captures the main features of the flow observed experimentally: 1) flow directed toward the spherical diatom along the direction normal to its surface, 2) compression of fluid streamlines near the regularized Stokeslet, 3) highest flow speeds around the regularized Stokeslet, and 4) zero flows at the diatom surface (Fig. 2 and *SI Appendix*, Fig. S3).

To determine the effect of these advective currents on nutrient availability to the diatom, we numerically solved the advection-diffusion equation $\mathbf{u} \cdot \nabla C = D \cdot C$ for the steady-state concentration of nutrients around the diatom surface. Here, $\mathbf{u} \cdot \nabla C$and $D\Delta C$ are, respectively, the advective and diffusive rates of change of the nutrient concentration field C (*SI Appendix*). We normalized the concentration field by its far-field value at large distances away from the diatom. At the diatom surface, the concentration is zero and reflects the assumption that nutrient absorption at the cell surface greatly exceeds transport rates of molecular diffusion (4, 7, 8). By Fick's law, a gradient in concentration yields a flux. The diatom nutrient uptake rate is the integral of the inward flux $I = \oint D\mathbf{n} \cdot \nabla C \, dS$ over the surface area of the diatom, where ∇C is the concentration gradient and $\mathbf{n}$ is the unit normal to the diatom surface. In the absence of advective flows, the nutrient concentration is governed by molecular diffusion only (Fig. 3*A*). The diffusive nutrient uptake I_d scales linearly with the diatom radius R, imposing serious limitations on diatom size (8, 35). In contrast, for a diatom sinking at Pe = 100 (Fig. 3*B* and *SI Appendix*, Figs. S1 and S2), the diffusive boundary layer gets thinner around most of the diatom, with only a plume or "tail" of nutrient depletion, characteristic of decaying marine snow (36), extending behind the sinking diatom. This constriction of the depletion zone enhances nutrient uptake to the sinking diatom by over threefold. When a diatom is in consortium with ciliated epibionts, the epibiont-induced flows change the concentration field around the diatom model (Figs. 2 *B* and *C* and 3*C* and *SI Appendix*, Fig. S3). We first considered the flow field induced by a pair of epibionts symmetrically attached at opposite poles of the diatom to ensure that forces and moments on the diatom are balanced, accounting only for the effect of ciliate-driven flows (*SI Appendix*, Table S3). The nutrient depletion zone is thinnest near the epibiont attachment locations on both sides of the diatom (Fig. 3*C*), and nutrient uptake is improved at a level that is comparable, even slightly higher than that of the sinking diatom.

To account for more ciliates on larger diatoms, we next considered the average flow field generated by N pairs of ciliates uniformly distributed along the diatom surface (*SI Appendix*, Table S4 and Fig. S4). Ciliates typically attach randomly on either or both sides of the diatom, often causing motion of the whole consortium. Mounting experimental and numerical evidence suggests that motion relative to the fluid is beneficial for both epibiont and diatom (21, 26, 37). However, statistics of attachment sites and ciliates-induced motions are currently lacking. We thus focused only on stationary configurations, because they provide a lower estimate of the benefits due to ciliate attachment. Specifically, to allow enough spacing between the ciliates, we considered the number of attached ciliates N to be equal to the surface area of the spherical diatom divided by four times the area enclosed by the circular crown of the ciliate. We followed a standard algorithm for distributing the ciliates uniformly on the diatom surface using an equal area partition of the spherical surface (*SI Appendix*, Fig. S4). For example, a diatom of radius $R = 100$ μm can readily support eight pairs of ciliates. Assuming identical ciliates, we computed the ciliate-generated flow field in three dimensions, and we averaged the three-dimensional flow around the axis of symmetry of the ciliate distribution. We used the averaged flow field to numerically calculate an axisymmetric concentration field around the diatom (Fig. 3*D*). The effects of axisymmetry and underlying uniform distribution of Stokeslets are reflected in the overall concentration field (*SI Appendix*, Fig. S4).

Sherwood Number. To place epibiont flows within a perspective that includes the more studied phenomenon of phytoplankton cell sinking, we assessed the benefits of epibiont-induced flows with reference to sinking for nutrient flux to the diatom. The cases illustrated in Fig. 3 *A–D* represent a diatom of radius $R = 100$ μm (*A*) in pure diffusive transport, (*B*) sinking, (*C*) in consortium with a single pair of epibionts, and (*D*) in consortia with eight pairs of uniformly distributed epibionts (highlighted in Fig. 3*E*). For this, we calculated the Sherwood number $Sh = I/I_d$ for a range of

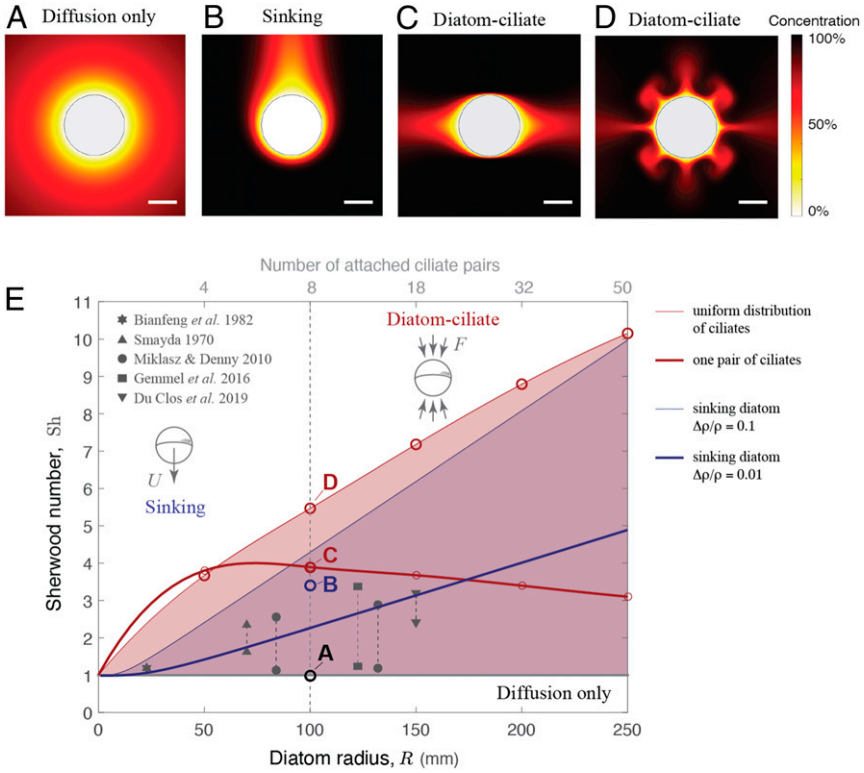

Fig. 3. Sherwood number and nutrient availability to the diatom *C. wailesii* in different hydrodynamic regimes. (*Top*) Results from numerical calculations of spatial dependence of the nutrient concentration around the spherical diatom model under (*A*) pure diffusion, (*B*) buoyancy-driven sinking at Pe = 100, and (*C*) microcurrents created by a single pair of ciliates *P. coscinodisci* (Stokeslets) attached symmetrically to both sides of the diatom. (*D*) Microcurrents created by eight pairs of ciliates uniformly distributed along the diatom surface. The dimensionless concentration is normalized by its far field value. Scale bars represent 100 microns in length. (*E*) Relationship between Sh and diatom radius due to advective microcurrents generated by the ciliate *P. coscinodisci* (thin red line) and theoretical upper limit of diatom *C. wailesii* sinking (thin blue line). In the diatom–ciliate model, Sh values are determined by the number of epibionts and the diatom radius. For epibionts that are uniformly distributed on the diatom surface (Sh shown in thin red line), the number of epibiont pairs is indicated on the top horizontal axis. The Sh values for a single pair of symmetrically opposed epibionts are shown in the thick red line. When sinking, Sh is determined by diatom radius and sinking rate, which in turn depends on density difference $\Delta\rho/\rho$ between the diatom and surrounding fluid. Sh = 1 corresponds to pure diffusion (Pe = 0). Sh numbers based on experimentally measured sinking rates are superimposed in gray symbols. For each diatom radius, two values of Sh are reported corresponding to the minimum and maximum measured sinking velocities.

diatom radius R. Sh is defined as the ratio of the total nutrient flux I (advective plus diffusive) normalized by the diffusive flux I_d; Sh = 1 for pure diffusion and Sh > 1 when advective currents enhance nutrient availability. For example, Sh = 5 indicates that the diatom nutrient uptake is fivefold that due to diffusion only. In Fig. 3*E*, we plotted Sh as a function R for 1) consortia with a single pair of epibionts and 2) consortia with increasing number N of epibiont pairs as R increases (*SI Appendix*, Tables S3 and S4); red circles of Fig. 3*E* are based on numerical computations and the solid red lines are obtained by a spline fit. For diatoms with uniform distributions of N pairs of ciliates; the values of Sh represent conservative upper estimates of the benefit of epibiont-induced flows to diatom nutrient uptake. A diatom of the same radius but smaller number of epibionts would lead to Sh values that lie within the region highlighted in red in Fig. 3*E*, between Sh =1 and the computed estimate. By way of comparison, we calculated a theoretical upper bound on Sh for sinking diatoms (thin blue line, Fig. 3*E*). This upper bound was obtained by noting that the velocity of a sinking diatom is $U_{sink} = 2gR^2\Delta\rho/9\eta$, where the acceleration due to gravity is $g = 9.8\ m{\cdot}s^{-2}$ and the difference in density $\Delta\rho$ between the diatom and the ambient fluid is set to the maximum reported value, $\Delta\rho = 100\ kg{\cdot}m^{-3}$ (8). At smaller density differences, Sh lies below the thin blue curve within the region highlighted in blue. The overlap between the red and blue regions indicates that, for a wide range of diatom sizes, similar enhancement in nutrient uptake can be achieved by either sinking or diatom–epibiont consortia.

To complete this analysis, we compiled a set of experimental measurements of diatom (*C. wailesii*) sinking velocities from the literature (16, 17, 38, 39), and we calculated the corresponding Pe and Sh numbers (*SI Appendix*, Table S5). Results are shown in gray symbols in Fig. 3*E*. For each diatom radius, we report two values of Sh corresponding to the minimum and maximum measured velocities. The results lie well in the overlap region of Sh values and demonstrate that combining with even a low number of epibionts allows nutrient enhancement that is of similar magnitude to that observed for sinking diatoms.

Discussion

Associations of the large nonmotile host and its smaller, motile epibiont can contribute to beneficial fluid dynamic outcomes for both members of the *Coscinodiscus–Pseudovorticella* consortia. Hydrodynamic effects on protists that use microcurrents to feed while attached to larger particles have been previously considered (19–22, 40, 41), so we concentrated here on alterations of nutrient availability to the larger diatom host cell. For a large diatom such as *C. wailesii*, microcurrent advection is a substantially more rapid mechanism of dissolved mass transport than diffusion (Fig. 3).

Advection by epibiont ciliary flows substantially thins diffusive boundary layers (Fig. 3*C* and *SI Appendix*, Fig. S3), allowing greater access to dissolved nutrients in waters surrounding the consortium.

The increased nutrient access due to epibiont-based advection is of a similar or greater magnitude than that due to diatom sinking without epibionts (Fig. 3*E*). Sinking allows a large diatom such as *C. wailesii* to create advective flows past itself (*SI Appendix*, Fig. S1) and thereby thin its diffusive boundary layer (*SI Appendix*, Fig. S2), resulting in higher nutrient flux rates than nonsinking cells (8, 17). Comparison of Sh values indicate that the relative advantages of either strategy—sinking or association with epibionts–depends on the diatom size and number of associated epibionts (Fig. 3 and *SI Appendix*, Fig. S2). The parameter values we used to derive these assessments (*SI Appendix*, Tables S1 and S2) are conservative, and we expect that the epibiont-induced impacts on nutrient uptake to the diatom are robust estimates. Under natural conditions, it appears that strategies of either sinking or consortia formation coexist and some phytoplankton species, such as *C. wailesii* (17, 24), employ either strategy in different circumstances.

Our model underscores the need for greater understanding of consortia formation and maintenance in nature. By placing epibionts in an axisymmetric arrangement on the host surface, the model balances forces generated by the epibionts around the host surface and eliminates clumps or random groups of epibionts, which could create both elevated flows (42) and unbalanced forces that result in translation or rotation of the whole consortium (e.g., *SI Appendix*, Movie S4). Such epibiont-generated motions would likely create transient flows that increase mass transfer rates (17, 21, 37) to a consortium. Hence, we expect our projections using balanced forces and established diffusive boundary layers to be conservative estimates of epibiont-generated nutrient benefits for diatoms in these consortia.

The hydrodynamic benefits of consortia formation between large cells and microcurrent-generating epibionts appear to be valuable, particularly in nutrient poor environments where nutrient diffusion rates influence phytoplankton community composition. This suggests a question—if consortia formation is mutually beneficial, why are they not more commonplace in nature? It is possible that the full extent of such marine relationships may be underappreciated (43–46) because associations are often ephemeral and difficult to sample with conventional approaches. For example, members of the *Coscinodiscus–Pseudovorticella* consortia separated within 30 min of collection and require a rapid research protocol. More broadly, a mutual benefit may not be enough to maintain a consistent symbiotic relationship. Evolution of mutually beneficial relationships between epibionts and their hosts face a variety of obstacles (47–50) that limit consortia evolution or lessen mutual benefits for the collaborators and their offspring (51). Potential loss of active photosynthetic area for diatom surfaces occupied by epibionts or removal of ciliates from productive regions on a sinking diatom both represent potential liabilities to members of *Coscinodiscus–Pseudovorticella* consortia. In response to a variety of conditions, protistan consortia have evolved a diverse spectrum of solutions (52–54) involving facultative partners, such as *Coscinodiscus–Pseudovorticella*, as well as obligate relationships, such as the diatom-ciliate consortia of *Chaetoceros coarctactus–Vorticella oceanica*. Both of the latter consortia are found in the same geographic region and often occur simultaneously (24). Although member identities and the nature of these relationships vary, hydrodynamic benefits such as those experienced by *Coscinodiscus–Pseudovorticella* consortia and other multicellular groups (35, 55) create a physical benefit that can serve as a foundation for the evolution of more complex relationships.

Materials and Methods

Assemblage Collection and Fluid Flow Measurements. Plankton samples containing *C.s wailesii* and their *P. coscinodisci* epibionts were collected with a 200 μm mesh net daily during between 9 and 16 May 2016 along the coastline of Ubatuba, Brazil. Within an hour following collection, diatom–ciliate consortia were hand sorted using a stereomicroscope and pipette. All selection and imaging work occurred in a temperature controlled (23 °C) room. Consortia were imaged with a Photron SA2 high-speed video camera mounted on an Olympus IX71 inverted microscope. Magnification varied between 20 and 60×, and the depths of field were 4.07, 2.08, and 0.93 μm at 20×, 40× and 60× magnifications, respectively. Frame rates for flow field analyses ranged from 500 to 1,000 fps. Cells were placed in 3.5 cm diameter fluorodishes (WPI Inc.) containing 3.5 to 4.0 mL of 0.7 μm filtered seawater so that cells could either float in suspension or sink to the dish bottom. Whole homogenized milk (0.25 to 0.5 mL) was added to ∼5 to 10% concentration for flow visualization. Suspended milk particles typically range between 0.3 and 3.0 μm and encourage high levels of consistent, flow generation by peritrich ciliates (56).

Species Identification and Nomenclature. Identification of *C. wailesii* (Coscinodiscales, Bacillariophyta) was based on morphological characters (valve dimensions and structure, chloroplast organization) and distribution patterns described for *C. wailesii* in surrounding Brazilian waters (23). Although we only observed cells in the 300 to 400 μm diameter range (that is, diatom radius $R = 150$ to 200 μm), laboratory studies (57) describe the full diameter range as 50 to 550 μm. Since average width of the *P. coscinodisci* ciliary crown was ∼40 μm, we used 100 to 500 μm as the range for model evaluations. *P. coscinodisci* (Ciliophora, Peritrichia) formed consortia with *C. wailesii* and matched recent descriptions from the region (24).

Fluid Flow Measurement. Two-dimensional PIV analysis quantified the fluid motions around the epibiont–host consortia. The velocity vectors of particles illuminated within microscope images were quantified from sequential images that were analyzed using a cross-correlation algorithm (LaVision Inc.). Image pairs were analyzed with shifting overlapping interrogation windows of decreasing size (64 × 64 pixels, then 32 × 32 pixels). Flow speeds for interrogation windows along transects through ciliate flow fields were averaged within crown and noncrown regions for each ciliate flow field. Reported values are averages and SDs of these measurements for replicate ($n = 8$) ciliates (Fig. 1*C*, *SI Appendix*). Kinematic measurements of cell locations and shapes were made using ImageJ (NIH).

Modeling Epibiont-Induced Flows. We developed a mathematical model of the flow field created by the ciliate around the diatom using a low-order representation of the diatom and the ciliate. Characteristic values of diatom radius and epibiont-induced velocities indicated that fluid viscosity is dominant, and the Stokes flow model is appropriate, similarly to sinking diatoms (*SI Appendix*, Table S1). Following common practice in studying sinking diatoms (8), we approximated the diatom as a sphere of radius R. We note that although these diatoms are cylindrical in form, spherical models best fit diatom sinking rates and do not significantly differ from those of a cylindrical model (58). To represent the flow generated by the ciliated ring of *P. coscinodisci*, we employed a simple model in which the details of the cilia length, beating frequency, and waveform are subsumed into a single averaged parameter, the force F that the ciliate exerts on the fluid (59, 60). Modeling applied forces (known as Stokeslets in viscous fluid) as a general flow solution (61) has been applied to other biological systems (62, 63) and is a common practice in studying ciliates attached to flat walls (26, 27). Here, we extend these models to ciliates attached to diatoms by representing the epibionts as regularized forces applied to the fluid domain outside a spherical diatom (34). Details of the model, as well as the sinking diatom model, can be found in *SI Appendix*.

Data Availability. All study data are included in the article and/or supporting information.

ACKNOWLEDGMENTS. We are grateful to Y. Garcia for help with organism sampling and sorting. E.A.K. is funded by NSF-2100209, NSF RAISE IOS-2034043 and NIH R01 HL 153622-01A1. R.M.L. is a CNPq research fellow (grant # 310642/2017-5). J.H.C. and J.O.D. are funded by Grant NSF-2100705.

1. P. Tréguer *et al.*, Influence of diatom diversity on the ocean biological carbon pump. *Nat. Geosci.* **11**, 27 (2018).
2. J.-Y. Park, J.-S. Kug, J. Bader, R. Rolph, M. Kwon, Amplified Arctic warming by phytoplankton under greenhouse warming. *Proc. Natl. Acad. Sci. U.S.A.* **112**, 5921–5926 (2015).
3. P. G. Falkowski, T. Fenchel, E. F. Delong, The microbial engines that drive Earth's biogeochemical cycles. *Science* **320**, 1034–1039 (2008).
4. H. C. Berg, E. M. Purcell, Physics of chemoreception. *Biophys. J.* **20**, 193–219 (1977).
5. J. P. Zehr, J. S. Weitz, I. Joint, How microbes survive in the open ocean. *Science* **357**, 646–647 (2017).

6. W. Munk, G. A. Riley, Absorption of nutrients by aquatic plants. *J. Mar. Res.* **11**, 215–240 (1952).
7. W. J. Pasciak, J. Gavis, Transport limitation of nutrient uptake in phytoplankton. *Limnol. Oceanogr.* **19**, 881–888 (1974).
8. L. Karp-Boss, E. Boss, P. Jumars, Nutrient fluxes to planktonic osmotrophs in the presence of fluid motion. *Oceanogr. Mar. Biol.* **34**, 71–108 (1996).
9. S. W. Chisholm, *Phytoplankton Size. Primary Productivity and Biogeochemical Cycles in the Sea* (Springer, 1992), pp. 213–237.
10. K. Mann, J. Lazier, *Dynamics of Marine Ecosystem* (Blakwell Science, 1991).
11. E. V. Armbrust, The life of diatoms in the world's oceans. *Nature* **459**, 185–192 (2009).
12. S. Malviya *et al*., Insights into global diatom distribution and diversity in the world's ocean. *Proc. Natl. Acad. Sci. U.S.A.* **113**, E1516–E1525 (2016).
13. D. M. Nelson, P. Tréguer, M. A. Brzezinski, A. Leynaert, B. Quéguiner, Production and dissolution of biogenic silica in the ocean: Revised global estimates, comparison with regional data and relationship to biogenic sedimentation. *Global Biogeochem. Cycles* **9**, 359–372 (1995).
14. C. S. Rousseaux, W. W. Gregg, Interannual variation in phytoplankton primary production at a global scale. *Remote Sens.* **6**, 1–19 (2014).
15. J. Bergkvist *et al*., Turbulence simultaneously stimulates small- and large-scale CO_2 sequestration by chain-forming diatoms in the sea. *Nat. Commun.* **9**, 3046 (2018).
16. P. Bienfang, P. Harrison, L. Quarmby, Sinking rate response to depletion of nitrate, phosphate and silicate in four marine diatoms. *Mar. Biol.* **67**, 295–302 (1982).
17. B. J. Gemmell, G. Oh, E. J. Buskey, T. A. Villareal, Dynamic sinking behaviour in marine phytoplankton: Rapid changes in buoyancy may aid in nutrient uptake. *Proc. R. Soc. B*, **283**, 20161126 (2016).
18. R. Margalef, *Ecologia* (Omega, Barcelona, 1974), p. 184.
19. K. K. Christensen-Dalsgaard, T. Fenchel, Increased filtration efficiency of attached compared to free-swimming flagellates. *Aquat. Microb. Ecol.* **33**, 77–86 (2003).
20. P. R. Jonsson, M. Johansson, R. W. Pierce, Attachment to suspended particles may improve foraging and reduce predation risk for tintinnid ciliates. *Limnol. Oceanogr.* **49**, 1907–1914 (2004).
21. A. Andersen, T. Kiørboe, The effect of tethering on the clearance rate of suspension-feeding plankton. *Proc. Natl. Acad. Sci. U.S.A.* **117**, 30101–30103 (2020).
22. H. Nguyen, M. A. R. Koehl, C. Oakes, G. Bustamante, L. Fauci, Effects of cell morphology and attachment to a surface on the hydrodynamic performance of unicellular choanoflagellates. *J. R. Soc. Interface* **16**, 20180736 (2019).
23. L. F. Fernandes, L. Zehnder-Alves, J. C. Bassfeld, The recently established diatom *Coscinodiscus wailesii* (Coscinodiscales, Bacillariophyta) in Brazilian waters. I: Remarks on morphology and distribution. *Phycol. Res.* **49**, 89–96 (2001).
24. F. Gómez, L. Wang, S. Lin, Morphology and molecular phylogeny of peritrich ciliate epibionts on pelagic diatoms: *Vorticella oceanica* and *Pseudovorticella coscinodisci* sp. nov. (Ciliophora, Peritrichia). *Protist* **169**, 268–279 (2018).
25. N. Liron, J. Blake, Existence of viscous eddies near boundaries. *J. Fluid Mech.* **107**, 109–129 (1981).
26. R. E. Pepper *et al*., A new angle on microscopic suspension feeders near boundaries. *Biophys. J.* **105**, 1796–1804 (2013).
27. R. E. Pepper, M. Roper, S. Ryu, P. Matsudaira, H. A. Stone, Nearby boundaries create eddies near microscopic filter feeders. *J. R. Soc. Interface* **7**, 851–862 (2009).
28. M. Rode, G. Meucci, K. Seegert, T. Kiørboe, A. Andersen, Effects of surface proximity and force orientation on the feeding flows of microorganisms on solid surfaces. *Phys. Rev. Fluids* **5**, 123104 (2020).
29. R. E. Pepper *et al*., The effect of external flow on the feeding currents of sessile microorganisms. *J. R. Soc. Interface* **18**, 20200953 (2021).
30. J. C. Nawroth *et al*., Motile cilia create fluid-mechanical microhabitats for the active recruitment of the host microbiome. *Proc. Natl. Acad. Sci. U.S.A.* **114**, 9510–9516 (2017).
31. M. Sleigh, D. Barlow, Collection of food by *Vorticella*. *Trans. Am. Microsc. Soc.* **95**, 482–486 (1976).
32. M. Nagai, M. Oishi, M. Oshima, H. Asai, H. Fujita, Three-dimensional two-component velocity measurement of the flow field induced by the *Vorticella picta* microorganism using a confocal microparticle image velocimetry technique. *Biomicrofluidics* **3**, 14105 (2009).
33. S. B. Penninck, R. M. Lopes, J. F. Lima, M. A. McManus, Thin layers in the coastal zone of Ubatuba, Brazil: Mechanisms of formation and dissipation. *Limnol. Oceanogr.* **66**, 558–574 (2021).
34. J. K. Wrobel, R. Cortez, D. Varela, L. Fauci, Regularized image system for Stokes flow outside a solid sphere. *J. Comput. Phys.* **317**, 165–184 (2016).
35. M. B. Short *et al*., Flows driven by flagella of multicellular organisms enhance long-range molecular transport. *Proc. Natl. Acad. Sci. U.S.A.* **103**, 8315–8319 (2006).
36. T. Kiorboe, H. Ploug, U. H. Thygesen, Fluid motion and solute distribution around sinking aggregates I: Small-scale fluxes and heterogeneity of nutrients in the pelagic environment. *Mar. Ecol. Prog. Ser.* **211**, 1–13 (2001).
37. S. Michelin, E. Lauga, Optimal feeding is optimal swimming for all Peclet numbers. *Phys. Fluids* **23**, 101901 (2011).
38. K. T. Du Clos, L. Karp-Boss, T. A. Villareal, B. J. Gemmell, *Coscinodiscus wailesii* mutes unsteady sinking in dark conditions. *Biol. Lett.* **15**, 20180816 (2019).
39. T. J. Smayda, The suspension and sinking of phytoplankton in the sea. *Oceanogr. Mar. Biol. Ann. Rev.* **8**, 353–414 (1970).
40. J. Carrias, C. Amblard, G. Bourdier, Protistan bacterivory in an oligomesotrophic lake: Importance of attached ciliates and flagellates. *Microb. Ecol.* **31**, 249–268 (1996).
41. J. B. Kirkegaard, R. E. Goldstein, Filter-feeding, near-field flows, and the morphologies of colonial choanoflagellates. *Phys. Rev. E* **94**, 052401 (2016).
42. M. Roper, M. J. Dayel, R. E. Pepper, M. A. Koehl, Cooperatively generated stresslet flows supply fresh fluid to multicellular choanoflagellate colonies. *Phys. Rev. Lett.* **110**, 228104 (2013).
43. C. de Vargas *et al*., Ocean plankton. Eukaryotic plankton diversity in the sunlit ocean. *Science* **348**, 1261605 (2015).
44. A. Gimmler, R. Korn, C. de Vargas, S. Audic, T. Stoeck, The Tara Oceans voyage reveals global diversity and distribution patterns of marine planktonic ciliates. *Sci. Rep.* **6**, 33555 (2016).
45. J. Decelle, S. Colin, R. A. Foster, *Photosymbiosis in Marine Planktonic Protists. Marine Protists* (Springer, 2015), pp. 465–500.
46. M. Nanajkar, V. Fernandes, K. Bogati, T. Chatterjee, Gregarious true-colonies of ciliate *Vorticella oceanica* on a chain forming diatom *Chaetoceros coarctatus*: Indicating change in the nature of association. *Symbiosis* **79**, 221–229 (2019).
47. J. Decelle *et al*., An original mode of symbiosis in open ocean plankton. *Proc. Natl. Acad. Sci. U.S.A.* **109**, 18000–18005 (2012).
48. E. Kazamia, K. E. Helliwell, S. Purton, A. G. Smith, How mutualisms arise in phytoplankton communities: Building eco-evolutionary principles for aquatic microbes. *Ecol. Lett.* **19**, 810–822 (2016).
49. M. A. Nowak, Five rules for the evolution of cooperation. *Science* **314**, 1560–1563 (2006).
50. M. Wahl, O. Mark, The predominantly facultative nature of epibiosis: Experimental and observational evidence. *Mar. Ecol. Prog. Ser.* **187**, 59–66 (1999).
51. E. T. Kiers, S. A. West, Evolutionary biology. Evolving new organisms via symbiosis. *Science* **348**, 392–394 (2015).
52. O. R. Anderson, Living together in the plankton: A survey of marine protist symbioses. *Acta Protozool.* **52**, 1–10 (2012).
53. J. R. Pratt, B. H. Rosen, Associations of species of *Vorticella* (Peritrichida) and planktonic algae. *Trans. Am. Microsc. Soc.* **102**, 48–54 (1983).
54. F. J. Vincent *et al*., The epibiotic life of the cosmopolitan diatom *Fragilariopsis doliolus* on heterotrophic ciliates in the open ocean. *ISME J.* **12**, 1094–1108 (2018).
55. C. A. Solari, S. Ganguly, J. O. Kessler, R. E. Michod, R. E. Goldstein, Multicellularity and the functional interdependence of motility and molecular transport. *Proc. Natl. Acad. Sci. U.S.A.* **103**, 1353–1358 (2006).
56. B. E. Zima-Kulisiewicz, A. Delgado, Synergetic microorganismic convection generated by *Opercularia asymmetrica* ciliates living in a colony as effective fluid transport on the micro-scale. *J. Biomech.* **42**, 2255–2262 (2009).
57. C. R. Tomas, *Identifying Marine Phytoplankton* (Academic Press, 1997).
58. K. Miklasz, M. Denny, Diatom sinkings speeds: Improved predictions and insight from a modified Stokes' law. *Limnol. Oceanogr.* **55**, 2513–2525 (2010).
59. J. Blake, S. Otto, Ciliary propulsion, chaotic filtration and a 'blinking' stokeslet. *J. Eng. Math.* **30**, 151–168 (1996).
60. T. Fenchel, "Protozon filter feeding" in *Progress in Protistology*, J. O. Corliss, D. J. Patterson, Eds. (Biopress Ltd., Bristol, England, 1986), vol. 65.
61. C. Oseen, *Neure Methoden und Ergebnisse in der Hydrodynamik* (Akademie Verlagsgesellschaft, Leipzig, 1927).
62. H. Jiang, T. R. Osborn, C. Meneveau, The flow field around a freely swimming copepod in steady motion. Part I: Theoretical analysis. *J. Plankton Res.* **24**, 167–189 (2002).
63. V. J. Langlois, A. Andersen, T. Bohr, A. W. Visser, T. Kiørboe, Significance of swimming and feeding currents for nutrient uptake in osmotrophic and interception-feeding flagellates. *Aquat. Microb. Ecol.* **54**, 35–44 (2009).